electronics

MDPI

Article

Improved Lv's Distribution for Noisy Multicomponent LFM Signals Analysis

Kai Yang [1,*], Xueshi Li [1], Yang Li [1] and Jibin Zheng [2,3]

[1] The 29th Research Institute of China Electronics Technology Group Corporation, Chengdu 610036, China; daxueshi01@126.com (X.L.); liyang_cetc@163.com (Y.L.)
[2] National Laboratory of Radar Signal Processing, Xidian University, Xi'an 710071, China; jbzheng@mail.xidian.edu.cn
[3] Collaborative Innovation Center of Information Sensing and Understanding, Xidian University, Xi'an 710071, China
* Correspondence: 17713583609@163.com

Abstract: This paper presents the improved Lv's distribution (ImLVD) for noisy multicomponent linear frequency-modulated (LFM) signals analysis, which is of significant importance in radar signal processing. Two goals of this paper are (i) to overcome drawbacks of the Lv's distribution (LVD), and (ii) to study mechanisms of the constant delay introduction. Theoretical comparisons in cross-term suppression, resolution, peak-to-sidelobe level, anti-noise performance and implementation are performed for the maximum likelihood (ML) method, Wigner–Hough transform (WHT), LVD, parameterized centroid frequency–chirp rate distribution (PCFCRD) and ImLVD. Based on theoretical comparisons and illustrative examples, superiorities of the ImLVD are demonstrated and several unclear mechanisms of the introduced constant delay are interpreted. Finally, three numerical examples are given to illustrate that, because of the high cross-term suppression, resolution, peak-to-sidelobe level and anti-noise performance without the non-uniform integration variable, the ImLVD is more suitable for noisy multicomponent LFM signals analysis.

Keywords: Lv's distribution; linear frequency-modulated signal; maximum likelihood method; Wigner–Hough transform

Citation: Yang, K.; Li, X.; Li, Y.; Zheng, J. Improved Lv's Distribution for Noisy Multicomponent LFM Signals Analysis. *Electronics* **2024**, *13*, 244. https://doi.org/10.3390/electronics13020244

Academic Editor: Massimiliano Pieraccini

Received: 16 November 2023
Revised: 24 December 2023
Accepted: 29 December 2023
Published: 5 January 2024

1. Introduction

Noisy multicomponent linear frequency-modulated (LFM) signals are often encountered in the field of radar signal processing, and its centroid frequency (CF) and chirp rate (CR) correspond to the velocity and acceleration [1,2]. Since the instantaneous frequency (IF) of the LFM signal varies linearly with time, time-frequency transforms, including linear transforms and bilinear transforms, have been widely used. The short-time Fourier transform and S-transform are typical linear transforms [3,4]. The linear transforms do not have the influence of the cross term, while high-frequency and time resolutions cannot be guaranteed simultaneously. In order to enhance the resolution, bilinear transforms are developed and the Wigner–Ville distribution (WVD) [5] is a typical bilinear transform. The WVD suffers from the serious influence of the cross term and several variations of it have been proposed, such as the modification of smoothed pseudo-WVD [6]. The optimized sparse fractional Fourier transform and combined use of discrete polynomial-phase transform and sparse fractional Fourier transform have been proposed to estimate LFM parameters [7,8]. Time–frequency transforms can serve as a basis for the radar signal synthesis, coding and detection, and related research is still going on [9–11].

The time–frequency transforms are based on one-dimensional energy integration and have a low anti-noise performance. In the field of radar signal processing, a high anti-noise performance is usually necessary [12]. Aiming to weaken this problem, another category of algorithms dealing with noisy multicomponent LFM signals is developed, known as the

CF–CR analysis technique (CFCRAT) [12]. In the past decades, many successful algorithms have been proposed. Based on the direct integration of the LFM signal, the maximum likelihood (ML) method [13], discrete Chirp–Fourier Transform [14], modified discrete Chirp–Fourier Transform [15] and fractional Fourier transform [16] are proposed. Because of the linearity, they do not have the influence of the cross term. Since the energy of each auto term of time–frequency transforms is concentrated into a line whose slope is related to the CR [17], some line integration-based algorithms are proposed. Representative algorithms include the Hough short-time Fourier transform [18], Hough-local polynomial periodogram [19], Wigner–Hough transform (WHT) [20] and modified-WVD [21]. Recently, the time-CR transforms similar to the time–frequency transforms are proposed and several integrated time-CR transforms are also developed in [22–29]. The CFCRAT is based on the two-dimensional energy integration and greatly enhances the anti-noise performance. Unfortunately, the past decades' research indicates that, no matter how the CFCRAT works in radar signal processing, some drawbacks are inherent and cannot be overcome [12,13,17–21], such as the low resolution, peak-to-sidelobe level (PSL) along the CR axis, etc.

Analyses and simulations in [12,17] indicate that, through the constant delay introduction, the recently reported Lv's distribution (LVD) further develops the CFCRAT and obtains superiorities in the cross-term suppression, resolution and anti-noise performance. The LVD has been applied in radar detection [30], imaging [31] and ultrasonic [32,33]. In 2017, we analyzed mechanisms of the constant delay introduction and proposed the parameterized centroid frequency–chirp rate distribution (PCFCRD) which obtains the higher cross-term suppression, CR resolution and anti-noise performance than the LVD [34]. Unfortunately, the PCFCRD is based on the time-CR transform and the integration variable in the integrant is non-uniform, which is not preferred in realistic applications [35]. The LVD is based on the time–frequency transform and can avoid the non-uniform integration variable. Therefore, if we base our work on mechanisms of the constant delay introduction obtained in [34] to improve the LVD, the proposed algorithm may have high cross-term suppression, CR resolution and anti-noise performance without the non-uniform integration variable.

In this paper, the improved LVD (ImLVD) is proposed for noisy multicomponent LFM signals analysis which is of significant importance in the field of radar signal processing. The ImLVD is based on mechanisms of the constant delay which is introduced in [34]. With theoretical analyses and illustrative examples, we demonstrate that, compared to the ML method, WHT, LVD and PCFCRD, the ImLVD has superiorities in resolution, cross-term suppression, PSL, anti-noise performance and implementation. In addition, several unclear mechanisms of the introduced constant delay are interpreted, including quantitative influences of the constant delay on the cross-term suppression, resolution, PSL and anti-noise performance. Finally, four examples are used to validate the practicality of the ImLVD.

The remainder of this paper is organized as follows. Section 2 gives a brief review of the LVD and presents the ImLVD. Theoretical comparisons and numerical illustrations are given in Section 3. In addition, this part discusses the selection criterion of the constant delay. In Section 4, with three examples, we demonstrate superiorities of the ImLVD in noisy multicomponent LFM signals analysis. Section 5 includes the conclusion and future work.

2. The ImLVD

2.1. Review of the LVD

In radar signal processing, the slow-time dimension of radar echoes of multiple maneuvering targets is usually modeled as multicomponent LFM signals [36]. In a noisy environment, multicomponent LFM signals analysis plays an important role in radar detection, imaging and recognition [21,34,35]. For noisy multicomponent LFM signals, the LVD further develops the CFCRAT and obtains superiorities in the resolution, cross-term

suppression and anti-noise performance [7,17,20]. In the following, we give a brief review of the LVD. The noisy multicomponent LFM signals can be expressed as

$$\begin{aligned} s(t) &= \sum_{p=1}^{\mathrm{P}} s_p(t) + n(t), -\tfrac{T}{2} \le t \le \tfrac{T}{2} \\ &= \sum_{p=1}^{\mathrm{P}} A_p \exp\left[j2\pi\left(a_{1,p}t + \tfrac{1}{2}a_{2,p}t^2\right)\right] + n(t) \end{aligned} \tag{1}$$

where $s_p(t)$ and $n(t)$ denote the pth LFM signal and zero mean complex white Gaussian noise of the power σ^2, respectively. P is the number of signal components. A_p, $a_{1,p}$ and $a_{2,p}$ denote the amplitude, CF (Hz) and CR (Hz/s) of the pth LFM signal, respectively. T denotes the integration time, and its unit is s.

The IF of the pth LFM signal is given by

$$\mathrm{IF}_p(t) = \frac{d\varphi_p(t)}{dt} = a_{1,p} + a_{2,p}t \tag{2}$$

where $\varphi_p(t) = a_{1,p}t + a_{2,p}t^2/2$ denotes the phase function.

Based on the format of the IF, a correlation function can be expressed as

$$R_1(t,\tau) = s\left(t + \frac{\tau}{2}\right)s^*\left(t - \frac{\tau}{2}\right), \tau \in \left\{-\frac{T}{2} \le t + \frac{\tau}{2}, t - \frac{\tau}{2} \le \frac{T}{2}\right\} \tag{3}$$

where τ and *, respectively, denote the lag variable and complex conjugation.

Based on the evolution of the IF with respect to time, the WVD [7], a time–frequency transform, is proposed as

$$\mathrm{WVD}(t,f) = \int_{\tau} R_1(t,\tau)\exp(-j2\pi f\tau)d\tau \tag{4}$$

where f denotes the frequency domain with respect to τ.

With $R_1(t,\tau)$ in (3) and $s(t)$ in (1), we have

$$\mathrm{WVD}(t,f) = \underbrace{\sum_{p=1}^{\mathrm{P}} K_p \mathrm{sinc}\left[\frac{T}{2}(f - a_{1,p} - a_{2,p}t)\right]}_{\text{the auto term}} + C_{\mathrm{WVD}}(t,f) + n_{\mathrm{WVD}}(t,f) \tag{5}$$

where K_p denotes the correlation amplitude. $C_{\mathrm{WVD}}(t,f)$ and $n_{\mathrm{WVD}}(t,f)$, respectively, denote the cross term and noise [7].

The auto term of the WVD concentrates along the line $f - a_{1,p} - a_{2,p}t = 0$, which follows the evolution of the IF with respect to time. The WVD only coherently integrates the energy along the τ axis. Consequently, $C_{\mathrm{WVD}}(t,f)$ and $n_{\mathrm{WVD}}(t,f)$ make it difficult to analyze noisy multicomponent LFM signals [20]. By employing the Hough transform, the WHT [20] is proposed as

$$\mathrm{WHT}(f,r) = \int_{\tau}\int_{t} R_1(t,\tau)\exp(-j2\pi f\tau - j2\pi r\tau t)dtd\tau \tag{6}$$

where r denotes the CR domain.

Substituting $R_1(t,\tau)$ and $s(t)$ into (6), we have

$$\mathrm{WHT}(f,r) = \underbrace{\sum_{p=1}^{\mathrm{P}} K'_p \mathrm{sinc}\left[\frac{T}{2}(f - a_{1,p})\right]\int_{t} \exp\left[j2\pi(r - a_{2,p})\tau t\right]dt}_{\text{the auto term}} + C_{\mathrm{WHT}}(f,r) + n_{\mathrm{WHT}}(f,r) \tag{7}$$

where K'_p denotes the amplitude. $C_{\mathrm{WHT}}(f,r)$ and $n_{\mathrm{WHT}}(f,r)$, respectively, denote the cross term and noise [20].

The auto term in (7) needs to be solved by the Fresnel function [26], because its integration variable t is different from τt in the integrant [26]. The WHT realizes two-dimensionally coherent energy integration, and each auto term peaks at $(a_{1,p}, a_{2,p})$. In order to further enhance the resolution, cross-term suppression and anti-noise performance, the authors of the reference [17] introduced a constant delay into the correlation function $R_1(t,\tau)$ and defined a new correlation function as

$$R_2(t,\tau) = s\left(t+\frac{\tau+\alpha}{2}\right)s^*\left(t-\frac{\tau-\alpha}{2}\right), \tau \in \left\{-\frac{T}{2} \le t+\frac{\tau+\alpha}{2}, t-\frac{\tau+\alpha}{2} \le \frac{T}{2}\right\} \quad (8)$$

where α denotes a constant delay. Note that the constant delay introduction is guaranteed by more samplings [17,34]. For example, if α = 1 s and T = 1 s, we need to sample data of 2 s to guarantee the introduction of the constant delay. However, more samplings do not mean more computational cost. We can refer to [17,34] for more details.

Based on the new correlation function $R_2(t,\tau)$ and the idea of the WHT, the LVD [17] is proposed as

$$\mathrm{LVD}(f,r) = \int_{\tau}\int_{t} R_2(t,\tau)\exp[-j2\pi f\tau - j2\pi r\beta(\tau+\alpha)t]dtd\tau \quad (9)$$

where β is a scaling factor and related to α, and $\beta\alpha = 1$ [17].

Considering the direct reading of the CR and the precision of the interpolation, the reference [17] sets optimal values of α and β to be both "1" for the LVD. Under such a condition, we substitute $R_2(t,\tau)$ and $s(t)$ into (9) and obtain

$$\mathrm{LVD}(f,r) = \underbrace{\sum_{p=1}^{\mathrm{P}} K''_p \mathrm{sinc}\left[\frac{T}{2}(f-a_{1,p})\right]\int_t \exp\left[j2\pi(r-a_{2,p})(\tau+1)t\right]dt}_{\text{the auto term}} + C_{\mathrm{LVD}}(f,r) + n_{\mathrm{LVD}}(f,r) \quad (10)$$

where K''_p denotes the amplitude. $C_{\mathrm{LVD}}(f,r)$ and $n_{\mathrm{LVD}}(f,r)$, respectively, denote the cross term and noise [17].

The auto term in (10) also needs to be solved by the Fresnel function [26] and peaks at $(a_{1,p}, a_{2,p})$. The difference between the WHT and LVD is the introduced constant delay α. Mathematical analyses and numerical simulations in [12,17] indicate that the introduced constant delay can significantly enhance the resolution, cross-term suppression and anti-noise performance.

In 2017, through mechanisms analysis of the introduced constant delay, the proposed PCFCRD indicated that the introduced constant delay should not be smaller than the integration time T [34]. However, the constant delay α of the LVD in (10) is fixed to 1s and it may perform badly in the CR resolution, anti-noise performance, cross-term suppression and PSL under $T > 1$ s. Note that, in radar detection and imaging, a long integration time, i.e., $T > 1$ s, is usually necessary to obtain a high Doppler resolution [21,37]. The PCFCRD outperforms the LVD in most aspects due to the appropriate constant delay, while it has the non-uniform integration variable which is not preferred in realistic applications [34,35]. By contrast, the LVD is based on the time–frequency transform rather than the time-CR transform of the PCFCRD and can avoid the non-uniform integration variable. In the following, we base our work on mechanisms of the introduced constant delay obtained in [34] to improve the LVD.

2.2. The Proposed ImLVD

By borrowing ideas of the LVD [17] and PCFCRD [34], we define a new correlation function

$$R_3(t,\tau) = s\left(t+\frac{\tau+h}{2}\right)s^*\left(t-\frac{\tau+h}{2}\right), \tau \in \left\{-\frac{T}{2} \le t+\frac{\tau+h}{2}, t-\frac{\tau+h}{2} \le \frac{T}{2}\right\} \quad (11)$$

where h denotes a constant delay and it satisfies $h \ge T$. By contrast, α in (8) used by the LVD is fixed to 1s. When $T > 1$ s, we have $\alpha < T$ and the LVD may perform badly in the CR resolution, anti-noise performance, cross-term suppression and PSL [17,34].

If the integration variable is the same as that in the integrant, the PSL, cross-term suppression and anti-noise performance will be enhanced [26]. By referring to this idea and using the new correlation function $R_3(t,\tau)$, we propose the ImLVD as

$$\mathrm{ImLVD}(f,r) = \int_{\tau}\int_{(\tau+h)t} R_3(t,\tau)\exp[-j2\pi f\tau - j2\pi r(\tau+h)t]d[(\tau+h)t]d\tau \quad (12)$$

Substituting $R_3(t,\tau)$ and $s(t)$ into (12), we obtain

$$\mathrm{ImLVD}(f,r) = \underbrace{\sum_{p=1}^{\mathrm{P}} K_p'''\,\mathrm{sinc}\left[\frac{T}{2}(f-a_{1,p})\right]\mathrm{sinc}\left[\frac{(T+h)^2}{8}(r-a_{2,p})\right]}_{\text{the auto term}} + C_{\mathrm{ImLVD}}(f,r) + n_{\mathrm{ImLVD}}(f,r) \quad (13)$$

where K_p''' denotes the amplitude. $C_{\mathrm{ImLVD}}(f,r)$ and $n_{\mathrm{ImLVD}}(f,r)$, respectively, denote the cross term and noise. It is easily seen from (13) that the ImLVD obtains the closed analytical formula and also peaks at $(a_{1,p}, a_{2,p})$. Details about the computation steps from (12) to (13) are given in Appendix A.

Compared to the LVD in (10), the ImLVD in (12) has two differences, including:

(i) The integration variable of the ImLVD is the same as that in the integrant, and the inner Fourier transform in (12) becomes a normal Fourier transform when we let $t' = (\tau+h)t$;

(ii) $h \ge T$ in the ImLVD in (12), while α is fixed to 1s in the LVD in (10) and $\alpha \le T$ when $T > 1$ s.

The following mathematical analyses and numerical simulations will demonstrate that these differences will bring the advantages below.

(i) The first difference guarantees the closed analytical formula of the ImLVD in (13), which helps the ImLVD weaken the serious PSL loss and enhance the cross-term suppression and anti-noise performance [26];

(ii) The second difference guarantees the resolution, high cross-term suppression, PSL and anti-noise performance of the ImLVD.

(iii) In addition, the ImLVD is based on the time–frequency transform and avoids the non-uniform integration variable. This allows the ImLVD to be implemented by the fast Fourier transform (FFT)- and inverse FFT (IFFT)-based chirp Z-transform (CZT) instead of the non-uniform FFT of the PCFCRD [17,34].

Illustrative Example 1. *Here, we use a numerical example to illustrate how the ImLVD works in the case of multicomponent LFM signals. Consider three noise-free LFM signals, Au1, Au2 and Au3. Signal parameters are listed in Table 1, and the constant delay h of the ImLVD is set to 2s. A1, A2 and A3 denote signal amplitudes. Figure 1a–c show simulations results. The amplitudes of the signal components are often different and vary with time [17]. In order to illustrate that the varying amplitudes do not have any influence on the ImLVD, we refer to [16] to set* $A_1 = A_2 = A_3 = \left(1/\pi^{1/4}\right)\exp\left(-t^2/2\right)$*, and Figure 1d shows the ImLVD under this condition. Comparing Figure 1c with Figure 1d, we can determine whether the varying amplitudes will have any influence on the ImLVD or not.*

Table 1. Signal Parameters.

Sampling Frequency F_s	**200 Hz**	**Signal Length N**	**400**
Parameters of *Au1*	$A_1 = 1$	$a_{1,1}$ = 40 Hz	$a_{2,1}$ = 38 Hz/s
Parameters of *Au2*	$A_2 = 1$	$a_{1,2}$ = 8 Hz	$a_{2,2}$ = 2 Hz/s
Parameters of *Au3*	$A_3 = 1$	$a_{1,3}$ = −36 Hz	$a_{2,3}$ = −28 Hz/s

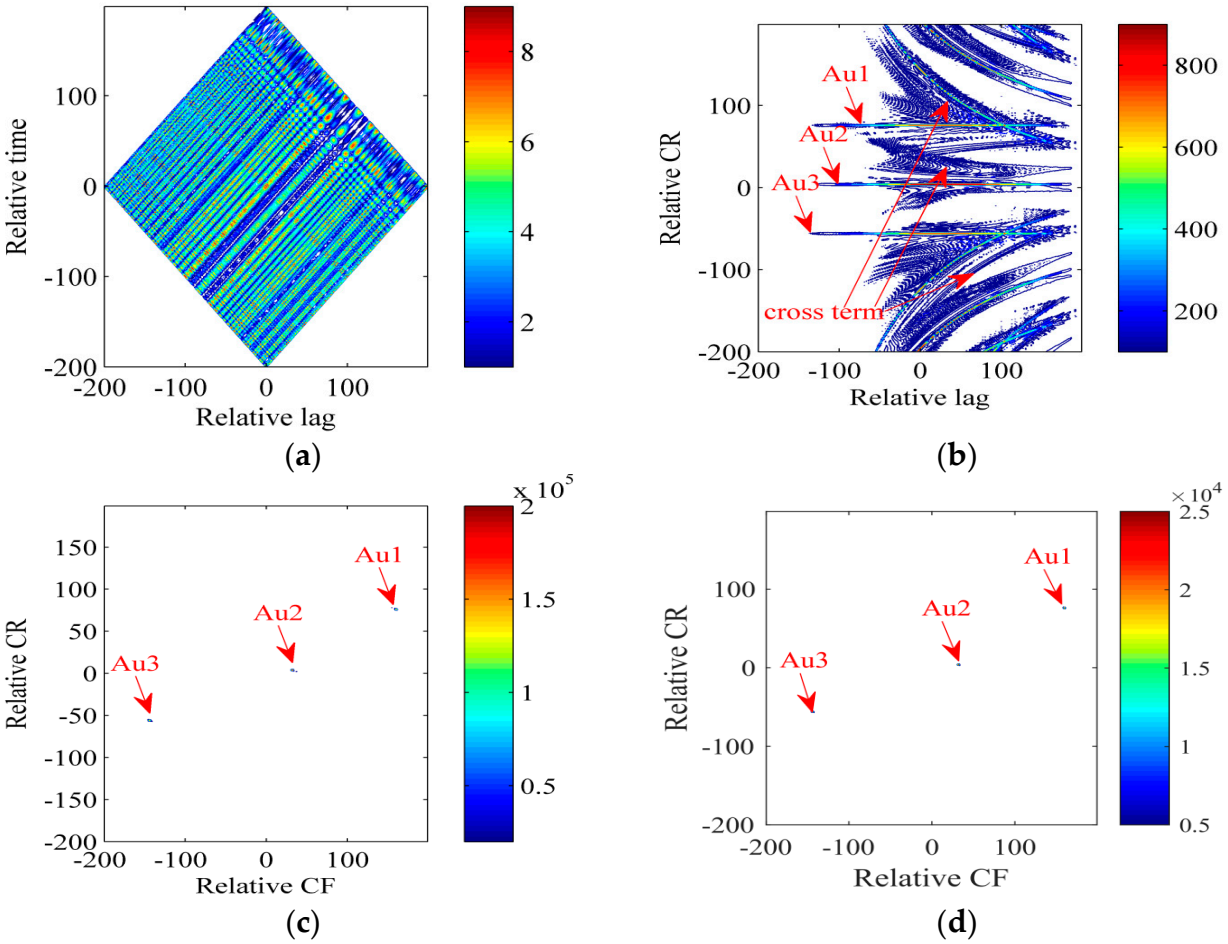

Figure 1. Illustration of ImLVD. (**a**) New correlation function defined in (11). (**b**) Result after inner integration in (12). (**c**) ImLVD. (**d**) ImLVD under $A_1 = A_2 = A_3 = \left(1/\pi^{1/4}\right)\exp(-t^2/2)$.

Figure 1a shows the new correlation function $R_3(t,\tau)$ which is defined in (11). We can find that the constant delay h does not increase the area of integrated signal, and the energy distribution is similar to that of the LVD [20]. Along the time axis in Figure 1a, we perform the Fourier transform with the integration variable $[(\tau + h)t]$, i.e., the inner integration in (12). The processing result is shown in Figure 1b, where the auto term and cross term coexist due to the bilinearity of the correlation function $R_3(t,\tau)$. The auto term peaks along $r = a_{2,p}$, while the cross term is distributed (will be demonstrated in Section 3.1). Performing the Fourier transform along the lag axis in Figure 1b, i.e., the outer integration in (12), we obtain the ImLVD in Figure 1c. As expected, the auto term of the ImLVD is integrated, while the cross term can be ignored compared with the auto term. Figure 1d shows the ImLVD under the varying amplitudes. Based on this result, we deduce that the varying amplitudes do not have any influence on the ImLVD.

3. Theoretical Comparisons and Numerical Illustrations

Generally, in realistic applications, the cross-term suppression, resolution, PSL, anti-noise performance and implementation determine the practicability of the signal analysis method [17,34]. In this section, with theoretical derivations and several numerical examples, we compare the ImLVD with the ML method, WHT, LVD and PCFCRD to demonstrate superiorities of the ImLVD. In addition, quantitative influences of the constant delay on the resolution, cross-term suppression, PSL and anti-noise performance are also studied.

3.1. Cross-Term Suppression

The ML method is linear and does not have the cross term, while the WHT, LVD, PCFCRD and ImLVD are bilinear and have the cross term. The analysis of the cross-term characteristic can demonstrate whether the cross term can accumulate as the auto term or not and give a more in-depth understanding of the cross-term suppression [17]. We analyze the cross-term characteristic through calculating cross terms of the WHT, LVD, PCFCRD and ImLVD [17,34].

With $s(t)$ in (1), WHT in (6), LVD in (9), PCFCRD in the reference [34] and ImLVD in (12), we calculate their cross terms as

$$C_{\mathrm{WHT}}(f,r)=\int_{\tau}\int_{t}\sum_{l=1}^{\mathrm{P}-1}\sum_{q=l+1}^{\mathrm{P}}A'_{lq}\underline{D'_{lq}(t,\tau)\cdot\exp\left[j2\pi\left(f-\nabla a_{1,lq}\right)\tau\right]}\cdot\underline{\exp\left[j2\pi\left(r-\nabla a_{2,lq}\right)\tau t\right]}dtd\tau \tag{14}$$

$$C_{\mathrm{LVD}}(f,r)=\int_{\tau}\int_{t}\sum_{l=1}^{\mathrm{P}-1}\sum_{q=l+1}^{\mathrm{P}}A''_{lq}\underline{D''_{lq}(t,\tau)\cdot\exp\left[j2\pi\left(f-\nabla a_{1,lq}\right)\tau\right]}\cdot\underline{\exp\left[j2\pi\left(r-\nabla a_{2,lq}\right)(\tau+1)t\right]}dtd\tau \tag{15}$$

$$C_{\mathrm{PCFCRD}}(f,r)=\int_{t}\int_{\tau}\sum_{l=1}^{\mathrm{P}-1}\sum_{q=l+1}^{\mathrm{P}}A'''_{lq}\underline{D'''_{lq}(t,\tau)\cdot\exp\left[j2\pi\left(f-\nabla a_{1,lq}\right)t\right]}\cdot\underline{\exp\left\{j2\pi\left(r-\nabla a_{2,lq}\right)\left[\left(\tau+\frac{h}{2}\right)^{2}+t^{2}\right]\right\}}d\tau dt \tag{16}$$

$$C_{\mathrm{ImLVD}}(f,r)=\int_{\tau}\int_{(\tau+h)t}\sum_{l=1}^{\mathrm{P}-1}\sum_{q=l+1}^{\mathrm{P}}A''''_{lq}\underline{D''''_{lq}(t,\tau)\cdot\exp\left[j2\pi\left(f-\nabla a_{1,lq}\right)\tau\right]}\cdot\underline{\exp\left[j2\pi\left(r-\nabla a_{2,lq}\right)(\tau+h)t\right]}d[(\tau+h)t]d\tau \tag{17}$$

where A'_{lq},A''_{lq},A'''_{lq} and A''''_{lq} denote amplitudes. $\nabla a_{1,lq}=\left(a_{1,l}+a_{1,q}\right)/2$, $\nabla a_{2,lq}=\left(a_{2,l}+a_{2,q}\right)/2$, $\Delta a_{1,lq}=a_{1,l}-a_{1,q}$ and $\Delta a_{2,lq}=a_{2,l}-a_{2,q}$. $D'_{lq}(t,\tau)=\cos\left\{2\pi\left[\Delta a_{1,lq}t+\left(\Delta a_{2,lq}/2\right)\left(t^{2}+\tau^{2}/4\right)\right]\right\}$, $D^{3}_{lq}(t,\tau)=\cos\left\{2\pi\left[\Delta a_{1,lq}t+\left(\Delta a_{2,lq}/2\right)\left[t^{2}+((\tau+1)/2)^{2}\right]\right]\right\}$, $D'''_{lq}(t,\tau)=\cos\left[2\pi\left(\Delta a_{1,lq}+\Delta a_{2,lq}t\right)(\tau+h/2)\right]$, $D''''_{lq}(t,\tau)=\cos\left\{2\pi\left[\Delta a_{1,lq}t+\left(\Delta a_{2,lq}/2\right)\left[t^{2}+((\tau+h)/2)^{2}\right]\right]\right\}$.

Analyses of (14), (15), (16) and (17) indicate that, if $D'_{lq}(t,\tau)$, $D''_{lq}(t,\tau)$, $D'''_{lq}(t,\tau)$ and $D''''_{lq}(t,\tau)$ do not exist; cross terms of the WHT, LVD, PCFCRD and ImLVD will seem like their auto terms and can be integrated. However, $D'_{lq}(t,\tau)$, $D''_{lq}(t,\tau)$, $D'''_{lq}(t,\tau)$ and $D''''_{lq}(t,\tau)$ do exist in their cross terms. As long as $a_{1,l}\neq a_{1,q}$ and $a_{2,l}\neq a_{2,q}$, cross terms of these four algorithms cannot accumulate as their auto terms.

By comparing $D'_{lq}(t,\tau)$ of the WHT with $D''_{lq}(t,\tau)$ of the LVD, $D'''_{lq}(t,\tau)$ of the PCFCRD and $D''''_{lq}(t,\tau)$ of the ImLVD, it is easy to find that the LVD, PCFCRD and ImLVD have additional disturbance factors, the constant delays "1 s" and "h". The authors of [17] have proved that, due to the constant delay introduction, the cross term depends on not only the auto term, but also the location of the auto term; that is, the constant delay introduction further disturbs the cross-term accumulation, and the cross-term strength -to-auto terms' peaks ratios, i.e., cross-term suppression [12,17,26,34], of the LVD, PCFCRD and ImLVD are smaller than that of the WHT. The ImLVD lets its integration variable be the same as that in the integrant, which helps the ImLVD further disturb the cross-term accumulation [26]. Therefore, the ImLVD may have the highest cross-term suppression.

Since the auto term peaks of these four algorithms are fixed, the cross-term strength can reflect the cross-term suppression [17,34]. Therefore, the following example uses the cross-term strength to reflect the cross-term suppression of these four algorithms.

Illustrative Example 2. *Consider three noise-free LFM signals, Bu1, Bu2 and Bu3. Signal parameters are listed in Table 2, and constant delays of the PCFCRD and ImLVD are set to 2 s. For each algorithm, we apply it to the noise-free multicomponent signals to obtain the simulation result* Θ*, and then apply it to each LFM signal to obtain simulation results* Θ_1*,* Θ_2 *and* Θ_3*. As a consequence, we obtain the cross-term strength as* $\Theta - \Theta_1 - \Theta_2 - \Theta_3$*. Figure 2a–d show the cross-term strength of the WHT, LVD, PCFCRD and ImLVD, respectively. Color bars in Figure 2 can indicate the cross-term strength. Auto term peaks of the WHT, LVD and PCFCRD are 80,000, and auto term peaks of the ImLVD are 160,000.*

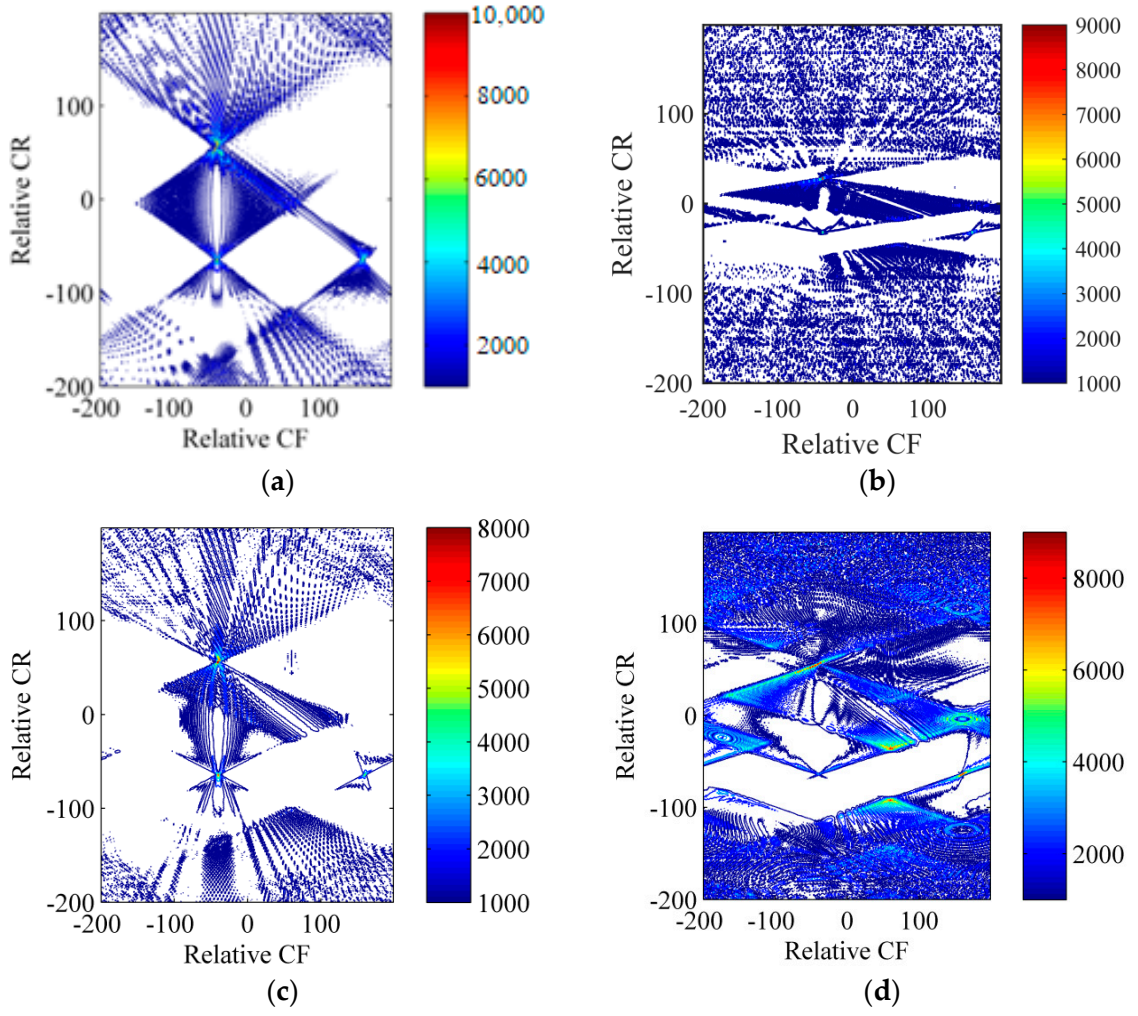

Figure 2. Comparison of cross-term strengths. (**a**) Cross-term strength of the WHT. (**b**) Cross-term strength of the LVD. (**c**) Cross-term strength of the PCFCRD. (**d**) Cross-term strength of the ImLVD.

Table 2. Signal Parameters.

Sampling Frequency F_s	**200 Hz**	**Signal Length** N	**400**
Parameters of *Bu1*	$A_1 = 1$	$a_{1,1} = 40$ Hz	$a_{2,1} = -32$ Hz/s
Parameters of *Bu2*	$A_2 = 1$	$a_{1,2} = -10$ Hz	$a_{2,2} = -32$ Hz/s
Parameters of *Bu3*	$A_3 = 1$	$a_{1,3} = -10$ Hz	$a_{2,3} = -28$ Hz/s

It is not difficult to find that this illustrative example considers the extreme condition $a_{2,1} = a_{2,2}$ and $a_{1,2} = a_{1,3}$ which benefits the cross-term accumulation. Under such an extreme condition, Figure 2 shows that cross terms of the WHT, LVD, PCFCRD and ImLVD are still distributed and their cross-term strength is much smaller than their auto-term peaks. The constant delay introduction further disturbs the cross-term accumulation. Therefore, the cross-term suppression of the LVD, PCFCRD and ImLVD is higher than that of the WHT. The ImLVD lets its integration variable be the same as that in the integrant, which helps the ImLVD further disturb the cross-term accumulation [26]. As expected, the ImLVD has the highest cross-term suppression in Figure 2.

3.2. Resolution

The Fourier transform is based on the process of interpolation, and the interpolation range determines the resolution [34]. Therefore, although the ML method, WHT and LVD cannot be given in closed analytical formulas, we still can obtain their resolutions based on their interpolation ranges. Formulas (18)–(22) give CF and CR resolutions of the ML method, WHT, LVD, PCFCRD and ImLVD.

$$\begin{cases} \delta_{\mathrm{ML}}(f) = \frac{2}{T} \\ \delta_{\mathrm{ML}}(r) = \frac{8}{T^2} \end{cases} \tag{18}$$

$$\begin{cases} \delta_{\mathrm{WHT}}(f) = \frac{2}{T} \\ \delta_{\mathrm{WHT}}(r) = \frac{8}{T^2} \end{cases} \tag{19}$$

$$\begin{cases} \delta_{\mathrm{LVD}}(f) = \frac{2}{T} \\ \delta_{\mathrm{LVD}}(r) = \frac{8}{(T+1)^2} \end{cases} \tag{20}$$

$$\begin{cases} \delta_{\mathrm{PCFCRD}}(f) = \frac{2}{T} \\ \delta_{\mathrm{PCFCRD}}(r) = \frac{8}{(T+h)^2} \end{cases} \tag{21}$$

$$\begin{cases} \delta_{\mathrm{ImLVD}}(f) = \frac{2}{T} \\ \delta_{\mathrm{ImLVD}}(r) = \frac{8}{(T+h)^2} \end{cases} \tag{22}$$

Formulas (18)–(22) indicate that, compared to the ML method and WHT, the LVD, PCFCRD and ImLVD have higher CR resolutions due to the constant delay introduction. In radar detection and imaging [17,21,34], the integration time T is usually larger than 1 s to guarantee the anti-noise performance and high azimuth resolution. Consequently, the CR resolutions of the PCFCRD and ImLVD are usually higher than that of the LVD. Since the resolution illustration is related with the PSL illustration, the illustrative example of the resolution will be given in the next subsection.

Remark 1. *Under $T < 1$ s, since $h = T < 1$ s, the CR resolution of the ImLVD will be lower than that of the LVD. Actually, we can also set $h \geq 1$ s under $T < 1$ s for the PCFCRD and ImLVD to guarantee its superiority in the CR resolution. However, (i) as discussed in Section 4, compared with $h \geq 1$ s, $h = T$ is more practical for the realistic application, and (ii) this paper aims to overcome drawbacks of the LVD under $T > 1$ s.*

3.3. PSL

The PSL is -13.3 dB for the sinc function and is -26.6 dB for the squared sinc function. Since the integration variable is different from that in the integrant, the ML method, WHT, LVD and PCFCRD have serious PSL losses along the CR axis [26]. In addition, for the LVD, as T is bigger than "1 s" and increases, the constant delay "1 s" has less and less influence on the resolution, and the sidelobe rises until it becomes a part of the mainlobe. Consequently, the PSL of the LVD along the CR is the same as that of the WHT under $T \leq 1$ s, while it is worse under $T > 1$ s. On the contrary, the integration variable of the

ImLVD is the same as that in the integrant, and $T = h$ guarantees the unchanged sidelobe along the CR axis.

$$\begin{cases} \mathrm{PSL}_{\mathrm{ML}}(f) = -13.3 \text{ dB} \\ \mathrm{PSL}_{\mathrm{ML}}(r) < -13.3 \text{ dB} \end{cases} \tag{23}$$

$$\begin{cases} \mathrm{PSL}_{\mathrm{WHT}}(f) = -26.6 \text{ dB} \\ \mathrm{PSL}_{\mathrm{WHT}}(r) < -26.6 \text{ dB} \end{cases} \tag{24}$$

$$\begin{cases} \mathrm{PSL}_{\mathrm{LVD}}(f) = -26.6 \text{ dB} \\ \mathrm{PSL}_{\mathrm{LVD}}(r) \leq \mathrm{PSL}_{\mathrm{WHT}}(r) \end{cases} \tag{25}$$

$$\begin{cases} \mathrm{PSL}_{\mathrm{PCFCRD}}(f) = -26.6 \text{ dB} \\ \mathrm{PSL}_{\mathrm{PCFCRD}}(r) = \mathrm{PSL}_{\mathrm{WHT}}(r) \end{cases} \tag{26}$$

$$\begin{cases} \mathrm{PSL}_{\mathrm{ImLVD}}(f) = -26.6 \text{ dB} \\ \mathrm{PSL}_{\mathrm{ImLVD}}(r) = -26.6 \text{ dB} \end{cases} \tag{27}$$

In (23)–(27), PSLs along the CR axis are derived with the continuous signal. However, in realistic applications, the discrete non-uniform interpolation along the CR axis will induce a small amount of PSL loss [24]. The actual PSLs of the ML method, WHT, PCFCRD and ImLVD along the CR axis are −8.785 dB, −17.57 dB, −17.57 dB and −23.3 dB, respectively. This conclusion can be found in references [17,26,34] and also can be demonstrated by the following illustrative examples. We rewrite Formulas (23)–(27) as

$$\begin{cases} \mathrm{PSL}_{\mathrm{ML}}(f) = -13.3 \text{ dB} \\ \mathrm{PSL}_{\mathrm{ML}}(r) = -8.785 \text{ dB} \end{cases} \tag{28}$$

$$\begin{cases} \mathrm{PSL}_{\mathrm{WHT}}(f) = -26.6 \text{ dB} \\ \mathrm{PSL}_{\mathrm{WHT}}(r) = -17.57 \text{ dB} \end{cases} \tag{29}$$

$$\begin{cases} \mathrm{PSL}_{\mathrm{LVD}}(f) = -26.6 \text{ dB} \\ \mathrm{PSL}_{\mathrm{LVD}}(r) \leq -17.57 \text{ dB} \end{cases} \tag{30}$$

$$\begin{cases} \mathrm{PSL}_{\mathrm{PCFCRD}}(f) = -26.6 \text{ dB} \\ \mathrm{PSL}_{\mathrm{PCFCRD}}(r) = -17.57 \text{ dB} \end{cases} \tag{31}$$

$$\begin{cases} \mathrm{PSL}_{\mathrm{ImLVD}}(f) = -26.6 \text{ dB} \\ \mathrm{PSL}_{\mathrm{ImLVD}}(r) = -23.3 \text{ dB} \end{cases} \tag{32}$$

Formulas (28)–(32) indicate that, compared with the ML method, WHT, LVD and PCFCRD, the ImLVD has the obvious superiority in the PSL along the CR axis. In the following, with two illustrative examples, T = 1 s and T > 1 s, we verify theoretical derivations of Sections 3.2 and 3.3.

Remark 2. *References* [17,34] *demonstrate that the constant delay introduction benefits the cross-term suppression, resolution and anti-noise performance, while they do not study the influence of the introduced constant delay on the PSL. Interested readers may ask: If the integration variables of the ML method, WHT and LVD are the same as their integrant variables, can they also eliminate the serious PSL loss along the CR axis? Our answer is "no". This is because* $\partial\xi(t,\tau)/\partial t$ *(where* $\xi(t,\tau)$ *denotes the integration variable) of the ML method, WHT and LVD cannot satisfy* $\partial\xi(t,\tau)/\partial t \geq 0$ *or* $\partial\xi(t,\tau)/\partial t \leq 0$*. This is not the focus of this paper and will be studied in another paper.*

Illustrative Example 3. *We consider a noise-free LFM signal Cu. The sampling frequency* F_s *is 200 Hz, and the signal length N is equal to 200. The signal parameters are set as follows:* $A_1 = 1$, $a_{1,1}$ *= 8 Hz,* $a_{2,1}$ *=2 Hz/s. Constant delays of the PCFCRD and ImLVD are set to 1 s. Figure 3a,b show resolutions and PSLs along the CF and CR axes, respectively.*

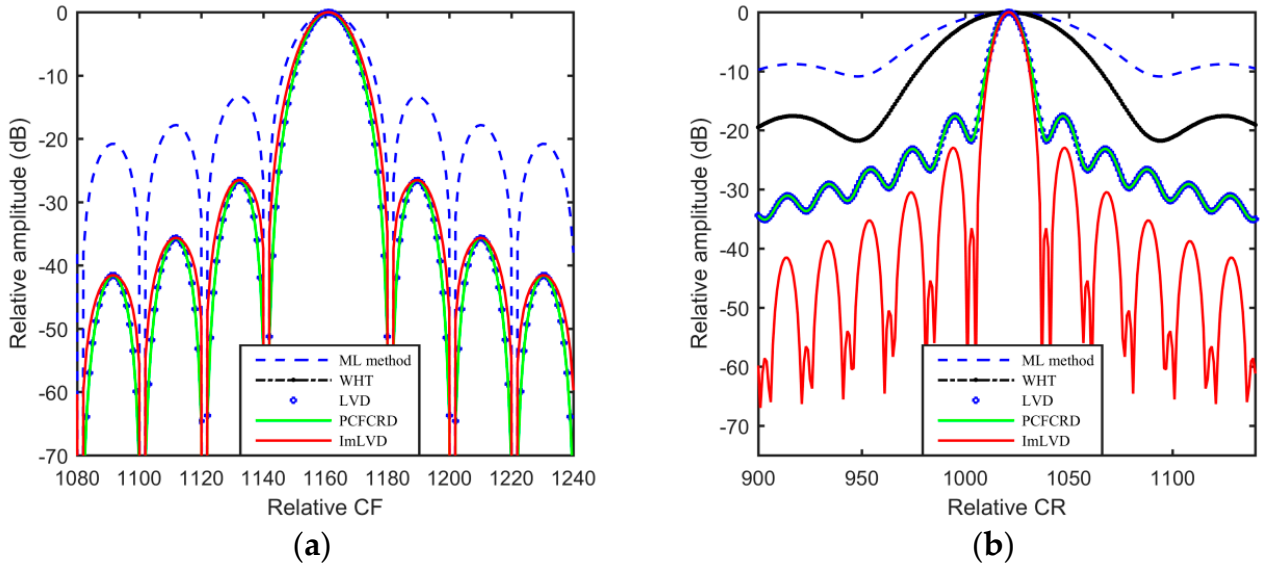

Figure 3. Comparisons of resolution and PSL under $T = 1$ s . (**a**) Comparisons along the CF axis. (**b**) Comparisons along the CR axis.

We obtain $\delta_{\mathrm{ML}}(f)$:$\delta_{\mathrm{WHT}}(f)$:$\delta_{\mathrm{LVD}}(f)$:$\delta_{\mathrm{ImLVD}}(f)$ as 1:1:1:1 and $\delta_{\mathrm{ML}}(r)$:$\delta_{\mathrm{WHT}}(r)$:$\delta_{\mathrm{LVD}}(r)$:$\delta_{\mathrm{ImLVD}}(r)$ as 4:4:1:1 by the simulation results shown in Figure 3. Simulation results of the resolution conform to the derived analytical formulas in (18)–(22). Compared to CR resolutions of the ML method and WHT, CR resolutions of the LVD, PCFCRD and ImLVD are enhanced due to the introduced constant delay. For the ML method, WHT, LVD and PCFCRD, their integration variables are different from those in the integrant and serious PSL losses along the CR axis exist. We obtain $\mathrm{PSL}_{\mathrm{ML}}(f)$:$\mathrm{PSL}_{\mathrm{WHT}}(f)$:$\mathrm{PSL}_{\mathrm{LVD}}(f)$:$\mathrm{PSL}_{\mathrm{ImLVD}}(f)$ as -13.3:-26.6:-26.6:-26.6 and $\mathrm{PSL}_{\mathrm{ML}}(r)$:$\mathrm{PSL}_{\mathrm{WHT}}(r)$:$\mathrm{PSL}_{\mathrm{LVD}}(r)$:$\mathrm{PSL}_{\mathrm{ImLVD}}(r)$ as -8.785:-17.57:-17.57:-23.3 by the simulation results shown in Figure 3. Simulation results of the PSL also conform to the derived analytical formulas in (28)–(32). This example demonstrates that (1) CR resolutions of the LVD, PCFCRD and ImLVD benefit from the constant delay introduction, and (2) the same integration variable and integrant variable help the ImLVD avoid the serious PSL loss along the CR axis.

Illustrative Example 4. *Here, we consider a noise-free LFM signal Du, and the signal lengthN is equal to 400. Constant delays of the PCFCRD and ImLVD are set to 2 s. Other simulation parameters are the same as those of* ***Illustrative Example 3****. Figures 4a and 4b, respectively, show resolutions and PSLs along the CF and CR axes.*

We obtain $\delta_{\mathrm{ML}}(f)$:$\delta_{\mathrm{WHT}}(f)$:$\delta_{\mathrm{LVD}}(f)$:$\delta_{\mathrm{ImLVD}}(f)$ as 1:1:1:1 and $\delta_{\mathrm{ML}}(r)$:$\delta_{\mathrm{WHT}}(r)$:$\delta_{\mathrm{LVD}}(r)$:$\delta_{\mathrm{ImLVD}}(r)$ as 1/4:1/4:1/9:1/16 with the simulation results shown in Figure 4, which conform to derived analytical formulas in (18)–(22). Meanwhile, we obtain $\mathrm{PSL}_{\mathrm{ML}}(f)$:$\mathrm{PSL}_{\mathrm{WHT}}(f)$:$\mathrm{PSL}_{\mathrm{LVD}}(f)$:$\mathrm{PSL}_{\mathrm{ImLVD}}(f)$ as -13.3:-26.6:-26.6:-26.6 and $\mathrm{PSL}_{\mathrm{ML}}(r)$:$\mathrm{PSL}_{\mathrm{WHT}}(r)$:$\mathrm{PSL}_{\mathrm{LVD}}(r)$:$\mathrm{PSL}_{\mathrm{ImLVD}}(r)$ as -8.785:-17.57:-11.92:-23.3. The simulation results of the PSL also conform to derived analytical formulas in (28)–(32). Under $T > 1$ s, as expected, the CR resolution of the LVD still benefits from the introduced constant delay, while its PSL along the CR axis has additional serious loss. Simulations in Figures 3 and 4 demonstrate that, compared to the ML method, WHT, LVD and PCFCRD, the ImLVD has superiorities in the resolution and PSL along the CR axis.

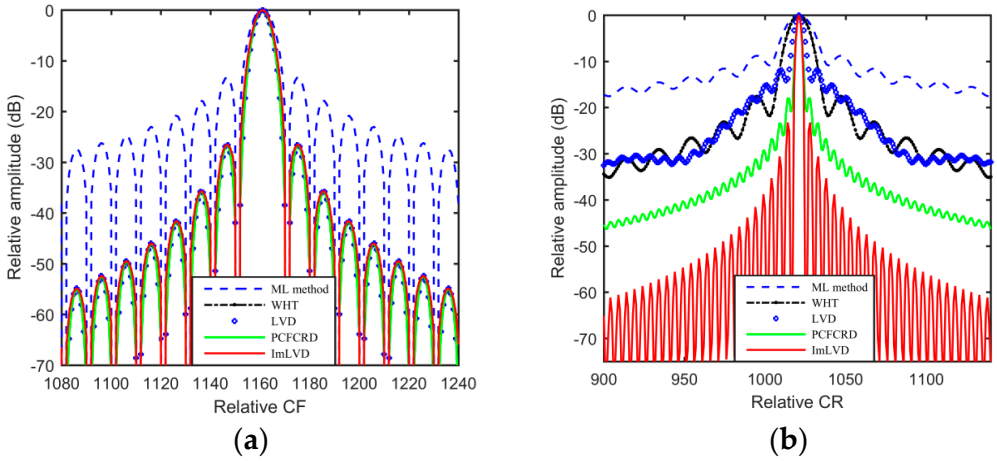

Figure 4. Comparisons of resolution and PSL under $T > 1$ s . (**a**) Comparisons along the CF axis. (**b**) Comparisons along the CR axis.

3.4. Anti-Noise Performance

This subsection focuses on the comparison of the anti-noise performance. With the discrete noisy LFM signal $s(m) = s_1(m) + n(m)$ ($m = -[N/2], -[N/2]+1, \ldots, [(N-1)/2]$ and the sampling interval is T_s), we first calculate the expect value and modulus square expect value at (f_0, r_0) which stands for the peak's coordinate of the ImLVD of the noiseless LFM signal. Then, a theoretical evaluation method is proposed and used to verify the high anti-noise performance of the ImLVD.

3.4.1. Expect Value at (f_0, r_0)

The ML method, WHT, LVD, PCFCRD and ImLVD can be applied to $s(m)$ and can take the expect values of ML(f_0, r_0), WHT(f_0, r_0), LVD(f_0, r_0), PCFCRD(f_0, r_0) and ImLVD(f_0, r_0). In radar detection and imaging, the integration time T is usually larger than 1s to guarantee the anti-noise performance and high azimuth resolution. Therefore, we consider $T > 1$ s and use the software "Wolfram Mathematica 13.1" to calculate expect values of ML(f_0, r_0), WHT(f_0, r_0), LVD(f_0, r_0), PCFCRD(f_0, r_0) and ImLVD(f_0, r_0) as

$$E[\mathrm{ML}(f_0, r_0)] = NA_1 \tag{33}$$

$$E[\mathrm{WHT}(f_0, r_0)] = \frac{N^2 A_1^2}{2} + N\sigma^2 \tag{34}$$

$$E[\mathrm{LVD}(f_0, r_0)] = \frac{N^2 A_1^2}{2} + \Psi\left(\sigma^2\right), \Psi\left(\sigma^2\right) \in \left(0, N\sigma^2\right) \tag{35}$$

$$E[\mathrm{PCFCRD}(f_0, r_0)] = \frac{N^2 A_1^2}{2} h \tag{36}$$

$$E[\mathrm{ImLVD}(f_0, r_0)] = \frac{N^2 A_1^2}{2} h \tag{37}$$

3.4.2. Modulus Square Expect Value at (f_0, r_0)

Applying the ML method, WHT, LVD, PCFCRD and ImLVD to $s(m)$, we take the modulus square expect value at (f_0, r_0). We also consider $T > 1$ s. By employing the software "Wolfram Mathematica" and the properties of the moment of zero mean complex Gaussian random variables, we calculate modulus square expect values of ML(f_0, r_0), WHT(f_0, r_0), LVD(f_0, r_0), PCFCRD(f_0, r_0) and ImLVD(f_0, r_0) as

$$E\left\{\left|\mathrm{ML}(f_0, r_0)\right|^2\right\} = N^2 A_1^2 + N\sigma^2 \tag{38}$$

$$E\left\{|\mathrm{WHT}(f_0,r_0)|^2\right\} = \frac{N^4A_1^4}{4} + \frac{3N^3A_1^2}{2}\sigma^2 + \frac{3N^2}{2}\sigma^4 \tag{39}$$

$$E\left\{|\mathrm{LVD}(f_0,r_0)|^2\right\} = \frac{N^4A_1^4}{4} + \Theta\left(\sigma^2\right) \tag{40}$$

$$E\left\{|\mathrm{PCFCRD}(f_0,r_0)|^2\right\} = h^2\left(\frac{N^4A_1^4}{4} + \frac{N^3A_1^2}{2}\sigma^2 + \frac{N^2}{2}\sigma^4\right) \tag{41}$$

$$E\left\{|\mathrm{ImLVD}(f_0,r_0)|^2\right\} = h^2\left(\frac{N^4A_1^4}{4} + \frac{N^3A_1^2}{2}\sigma^2 + \frac{N^2}{2}\sigma^4\right) \tag{42}$$

where $\Theta(\sigma^2) \in \left(\frac{N^3A_1^2}{2}\sigma^2 + \frac{N^2}{2}\sigma^4, \frac{3N^3A_1^2}{2}\sigma^2 + \frac{3N^2}{2}\sigma^4\right)$.

If we separately use the expect value or modulus square expect value as a criterion to determine the anti-noise performance, it is difficult to directly tell which algorithm is better. References [17,20,28] use the output signal-to-noise ratios (SNRs) to evaluate the anti-noise performance, while analyses in the following ***Remark 3*** show that this also cannot work. Interested readers may ask why. This is because they ignore the fact that the integrations after the bilinear algorithms, such as the WHT, LVD and ImLVD, take the form of energies of the signal plus noise, while the integrations after the linear algorithms, such as the ML method, take the form of amplitudes of the signal plus noise. Based on this understanding, we propose to use the expect value of the bilinear algorithm and the modulus square expect value of the linear algorithm to theoretically evaluate the anti-noise performance. By using $E[\mathrm{WHT}(f_0,r_0)]$ in (34), $E[\mathrm{LVD}(f_0,r_0)]$ in (35), $E[\mathrm{PCFCRD}(f_0,r_0)]$ in (36), $E[\mathrm{ImLVD}(f_0,r_0)]$ in (37) and $E\left\{|\mathrm{ML}(f_0,r_0)|^2\right\}$ in (38), we determine that the PCFCRD and ImLVD have a higher anti-noise performance than the other three algorithms. Reference [26] has indicated that, if the integration variable is the same as that in the integrant, the anti-noise performance will be enhanced. Therefore, the ImLVD has the highest anti-noise performance among these five algorithms.

Remark 3. *References* [17,20,28] *use the output signal-to-noise ratios (SNRs) to evaluate the integration SNR gain. We take the WHT as an example, and its output SNR is defined as*

$$SNR_{out,\mathrm{WHT}} = \frac{|\mathrm{WHT}_{s_1}(f_0,r_0)|^2}{\mathrm{var}\{\mathrm{WHT}_{s_n}(f_0,r_0)\}} \tag{43}$$

where var$\{\bullet\}$ denotes the variance. $\mathrm{WHT}_{s_1}(f_0,r_0)$ denotes the WHT of the signal only. $\mathrm{WHT}_{s_n}(f_0,r_0)$ *denotes the WHT of the signal plus noise.*

Based on (34), (37), (39), (42) and (43), we calculate output SNRs of the WHT and ImLVD as

$$SNR_{out,\mathrm{WHT}} = \frac{N^2A_1^4}{2NA_1^2\sigma^2 + 2\sigma^4} \tag{44}$$

$$SNR_{out,\mathrm{ImLVD}} = \frac{N^2A_1^4}{2NA_1^2\sigma^2 + 2\sigma^4} \tag{45}$$

Obviously, although the ImLVD has the obvious superiority in the anti-noise performance compared to the WHT, the evaluation method "output SNR" reveals that the WHT and ImLVD have the same output SNR.

Illustrative Example 5. *Consider the noisy LFM signal Eu. The sampling frequency* F_s *is 100 Hz and the signal length N is equal to 600. The signal parameters are set as follows:* $A_1 = 1$, $a_{1,1}$ *= 16 Hz,* $a_{2,1}$ *= 44 Hz/s. Constant delays of the PCFCRD and ImLVD are set to 6s. The tested SNRs-in are* SNR_{in} *= [−18 dB:1 dB:−12 dB], and 1000 trials are performed for each* SNR_{in}*. The measurement given in (46) is used to compare the anti-noise performance* [37] *. The SNR-out*

of the matched filter corresponds to $\mathrm{SNR}_{\mathrm{out}} = 10\log_{10} NA_1^2/\sigma^2$. Figure 5*a gives the integral SNR-in- SNR-out comparison, while* Figure 5*b gives the zoomed-in plot of [−15 dB:1 dB:−12 dB] in Figure* 5*a.*

$$SNR_{out} = 10\log_{10}\frac{A_1^2}{N\sigma^2}\left\{\left|\sum_{m=-\frac{N}{2}}^{\frac{N}{2}-1} s(m)\exp\left[-j2\pi a'_{1,1}mT_s\prime j2\pi\frac{a'_{2,1}}{2}(mT_s)^2\right]\right|_{\max}\right\}^2 \quad (46)$$

where $a'_{1,1}$ *and* $a'_{2,1}$ *are estimations of* $a_{1,1}$ *and* $a_{2,1}$ *with the peak detection technique, respectively.*

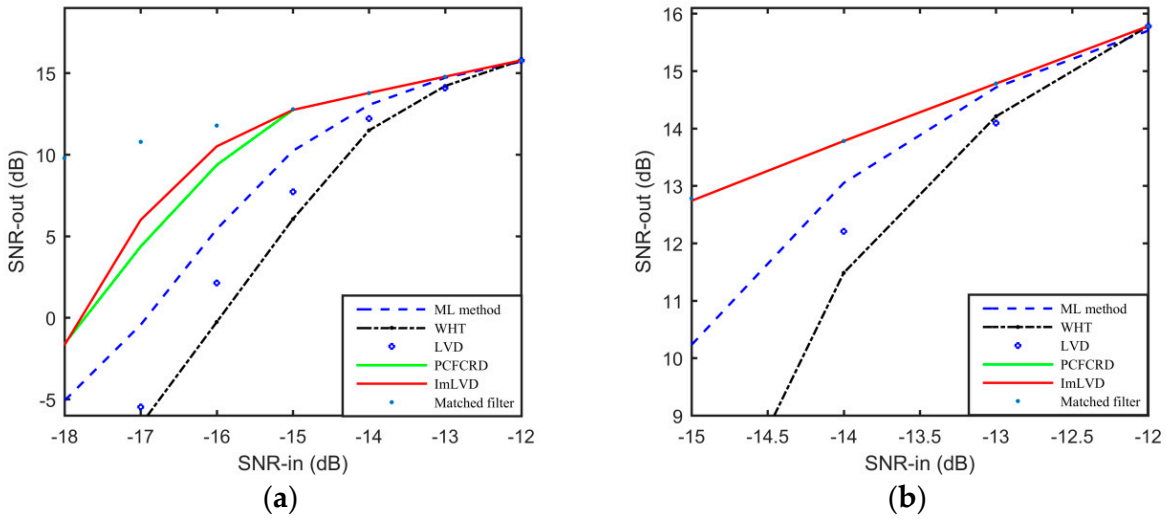

Figure 5. Comparison of the integration SNR gain. (**a**) Integral SNR-in- SNR-out comparison. (**b**) Zoomed-in plot of [−15 dB:1 dB:−12 dB] in Figure 5a.

As expected, the ImLVD has a higher anti-noise performance than the other four algorithms. Figure 5a,b show that the ImLVD and PCFCRD [12] are almost coincident with the matched filter when $\mathrm{SNR}_{\mathrm{in}} \geq -15$ dB, while the threshold $\mathrm{SNR}_{\mathrm{in}}$ is −13 dB for the ML method [13] and −12 dB for the other two algorithms. Based on the above analyses, we know that, if T is close to 1s, the anti-noise performance of the LVD [34] will be close to that of the ImLVD, while if T is much larger than 1s, the LVD will obtain a similar anti-noise performance as the WHT [20]. Thus, in Figure 5, the anti-noise performance of the LVD is close to that of the WHT and lower than that of the ML method, PCFCRD and ImLVD.

3.5. Implementation

As with the LVD, the ImLVD can be implemented by using the FFT- and IFFT-based chirp Z-transform (CZT), which is presented in Appendix A. Figure 6 shows the implementation flowchart of the ImLVD. With analyses of the implementation, we obtain that the computational cost of the ImLVD is in the order of $O(N^2\log_2 N)$. The ML method and WHT are based on the brute-force searching of the CF and CR. To guarantee the same estimation ranges of the CF and CR, we assume that the number of searching is N for both parameters. Under this assumption, computational costs of the ML method and WHT are both in the order of $O(N^3)$. In the reference [34], we use the non-uniform FFT to speed up the implementation of the PCFCRD, and its computational cost is also in the order of $O(N^2\log_2 N)$. However, the PCFCRD is based on the time-CR transform, and the integration variable in the integrant is non-uniform, which is not preferred in realistic applications [35]. Table 3 lists the computational costs of these five algorithms.

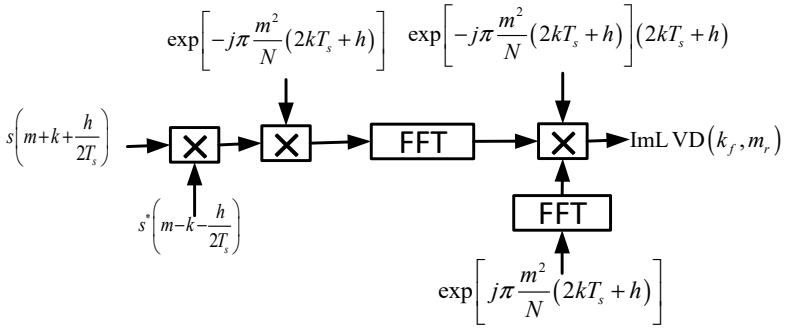

Figure 6. Implementation flowchart of the ImLVD.

Table 3. Computational Cost.

Algorithm	ML Method	WHT	LVD	PCFCRD	ImLVD
Computational cost	$O(N^3)$	$O(N^3)$	$O(N^2 \log_2 N)$	$O(N^2 \log_2 N)$	$O(N^2 \log_2 N)$

Remark 4. *Aforementioned computation cost analyses of the ML method and WHT are based on their original implementation methods. The references* [14,15,21] *have developed fast implementation methods for the ML method and WHT, and their computational costs are also in the order of* $O(N^2 \log_2 N)$. *Under such condition, these five algorithms require similar computational costs.*

Remark 5. *For the LFM signal, the ideal energy representation along the CR dimension takes the form of the sinc function in the CF–CR domain. Theoretical analyses and numerical simulations indicate that two differences between the LVD and ImLVD let the ImLVD take the form of the sinc function along the CR dimension. In other word, along the CR dimension, the energy of the ImLVD is more concentrated than that of the LVD. In addition, based on implementation details in Appendix A, we can find that two differences between the LVD and ImLVD are both realized with linear operations. Therefore, the ImLVD may enhance properties of the LVD, and the inverse ImLVD can also be defined as the inverse LVD. We can refer to [17,34] for more details.*

3.6. Constant Delay Selection Criterion

Theoretical comparisons in Section 3 reveal that the constant delay is related with the cross-term suppression, resolution, PSL and anti-noise performance. In this section, the constant delay selection criterion will be discussed.

Analytical formulas (14)–(22) indicate that the constant delay benefits the cross-term strength reduction and CR resolution. Analytical formulas (27), (32) and (37) indicate that, when the constant delay $h \geq T$, the anti-noise performance of the ImLVD achieves its optimum and the serious PSL loss along the CR axis can be eliminated. As we know, a large h means a large signal length, while the signal length is finite in realistic applications. Therefore, considering the cross-term suppression, resolution, PSL, anti-noise performance and actual signal length, we set

$$h = T \tag{47}$$

Remark 6. *For the LVD proposed in the reference [17], the selection criterion of the constant delay aims to guarantee that, (1) no interpolation is required along the scaled time axis and both sides of the scaled time axis are symmetrical, and (2) the CR value can be directly read from the CF–CR plane. By contrast, the selection criterion discussed here considers the interpolation, cross-term suppression, resolution, PSL, anti-noise performance, signal length and direct reading of the CR value. The selection criterion discussed here is more practical. For more details about the selection, we can refer to references [12,17,37].*

4. Numerical Simulations

In this section, we use three numerical examples to demonstrate the practicability of the ImLVD. These three numerical examples are the adjacent LFM signals separation, LFM signals with different amplitudes (of large differences) and noisy multicomponent LFM signals, which are representative scenarios existing in radar detection and imaging [17,30,31,34,35].

4.1. Adjacent LFM Signals Separation

The cross-term suppression, resolution and PSL jointly determine the adjacent LFM signals separation. In the following, we use the ***Numerical Example 1*** to illustrate the superiority of the ImLVD in the adjacent LFM signals separation.

Numerical Example 1 *Here, we consider three adjacent LFM signals, denoted by Fu1, Fu2 and Fu3. Signal parameters are listed in Table 4, and constant delays of the PCFCRD and ImLVD are set to 2s. The ML method, WHT, LVD, PCFCRD and ImLVD are applied to the data. Simulation results are shown in Figure 7 (X axis, Y axis and Z axis represent the Relative CF, Relative CR and Amplitude, respectively) and the part marked with the red ellipse is zoomed.*

Table 4. Signal Parameters.

Sampling Frequency F_s	**256 Hz**	**Signal Length N**	**512**
Parameters of *Fu1*	$A_1 = 1$	$a_{1,1} = -0.5$ Hz	$a_{2,1} = 0$ Hz/s
Parameters of *Fu2*	$A_2 = 1$	$a_{1,2} = 1$ Hz	$a_{2,2} = -0.5$ Hz/s
Parameters of *Fu3*	$A_3 = 1$	$a_{1,3} = 0.5$ Hz	$a_{2,3} = 0.5$ Hz/s

The ML method has low PSL and resolution, and the WHT has low cross-term suppression, resolution and PSL. The LVD introduces the constant delay "1s" to increase the resolution and cross-term suppression, while its PSL is not improved. The PCFCRD also encounters the serious PSL loss along the CR axis. Compared to the ML method, WHT and LVD, the ImLVD has obvious superiorities in the resolution, cross-term suppression and PSL. Consequently, in Figure 7, only the ImLVD can separate *Fu1*, *Fu2* and *Fu3* successfully.

4.2. LFM Signals with Different Amplitudes (of Large Differences)

The ImLVD is bilinear, and the cross term does exist. Under LFM signals with different amplitudes (of large differences), auto terms of weak LFM signals may be submerged in the residual cross terms generated by the strong LFM signals. In this subsection, we use a numerical example to demonstrate that the ImLVD has an obvious superiority under this situation.

Numerical Example 2. *Four LFM signals, denoted by Gu1, Gu2, Gu3 and Gu4, are considered. Signal parameters are listed in Table 5, and constant delays of the PCFCRD and ImLVD are set to 2 s. Processing results by the ML method, WHT, LVD, PCFCRD and ImLVD are shown in Figure 8, where the part marked with the red ellipse is zoomed.*

Table 5. Signal Parameters.

Sampling Frequency F_s	**256 Hz**	**Signal Length N**	**512**
Parameters of *Gu1*	$A_1 = 1$	$a_{1,1} = -1$ Hz	$a_{2,1} = -2$ Hz/s
Parameters of *Gu2*	$A_2 = 0.8$	$a_{1,2} = 1$ Hz	$a_{2,2} = 2$ Hz/s
Parameters of *Gu3*	$A_3 = 0.4$	$a_{1,3} = 0.5$ Hz	$a_{2,3} = 0.5$ Hz/s
Parameters of *Gu3*	$A_4 = 0.2$	$a_{1,3} = -8$ Hz	$a_{2,3} = -20$ Hz/s

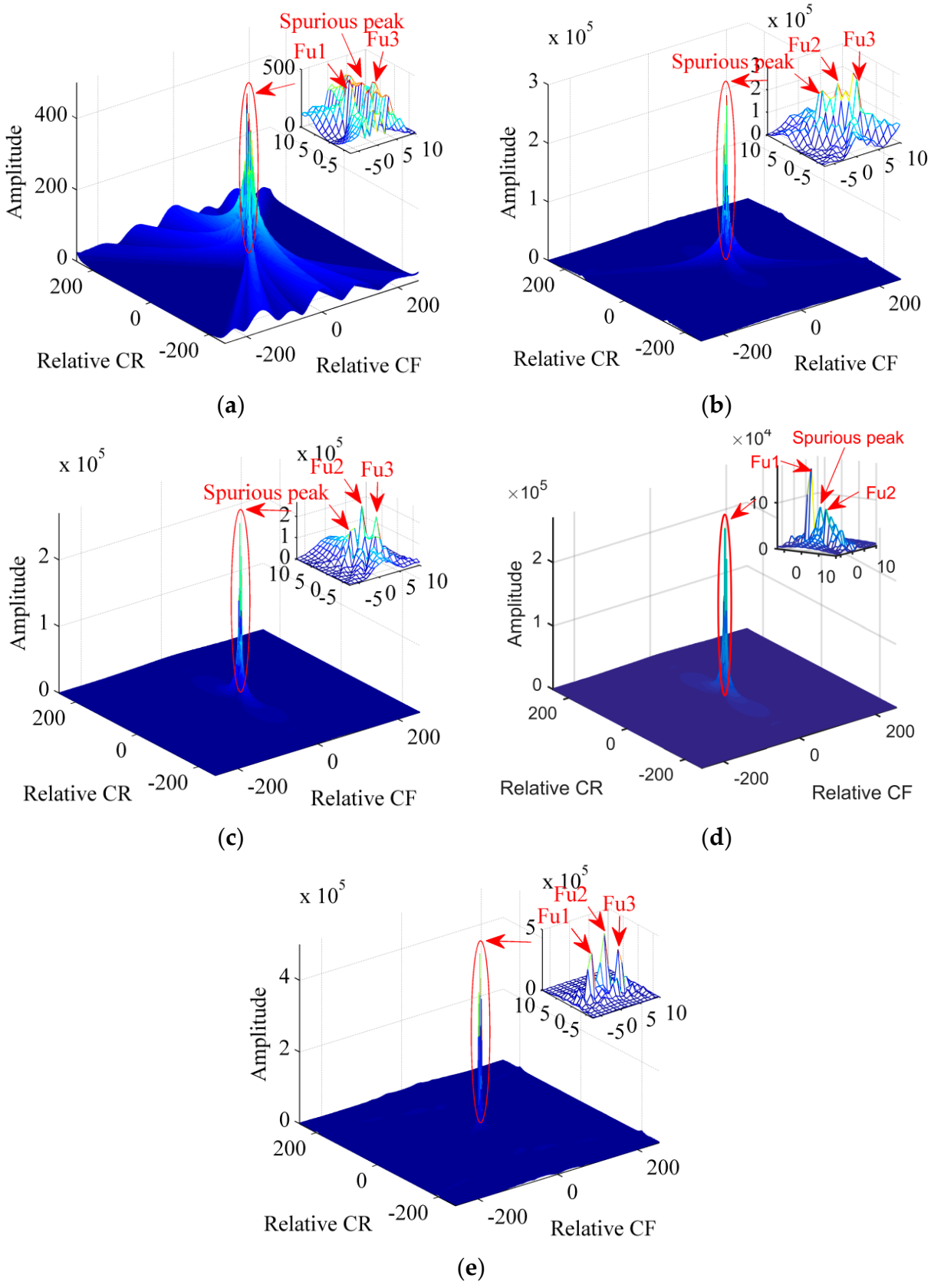

Figure 7. Adjacent LFM signals separation. (**a**) Result of the ML method. (**b**) Result of the WHT. (**c**) Result of the LVD. (**d**) Result of the PCFCRD. (**e**) Result of the ImLVD.

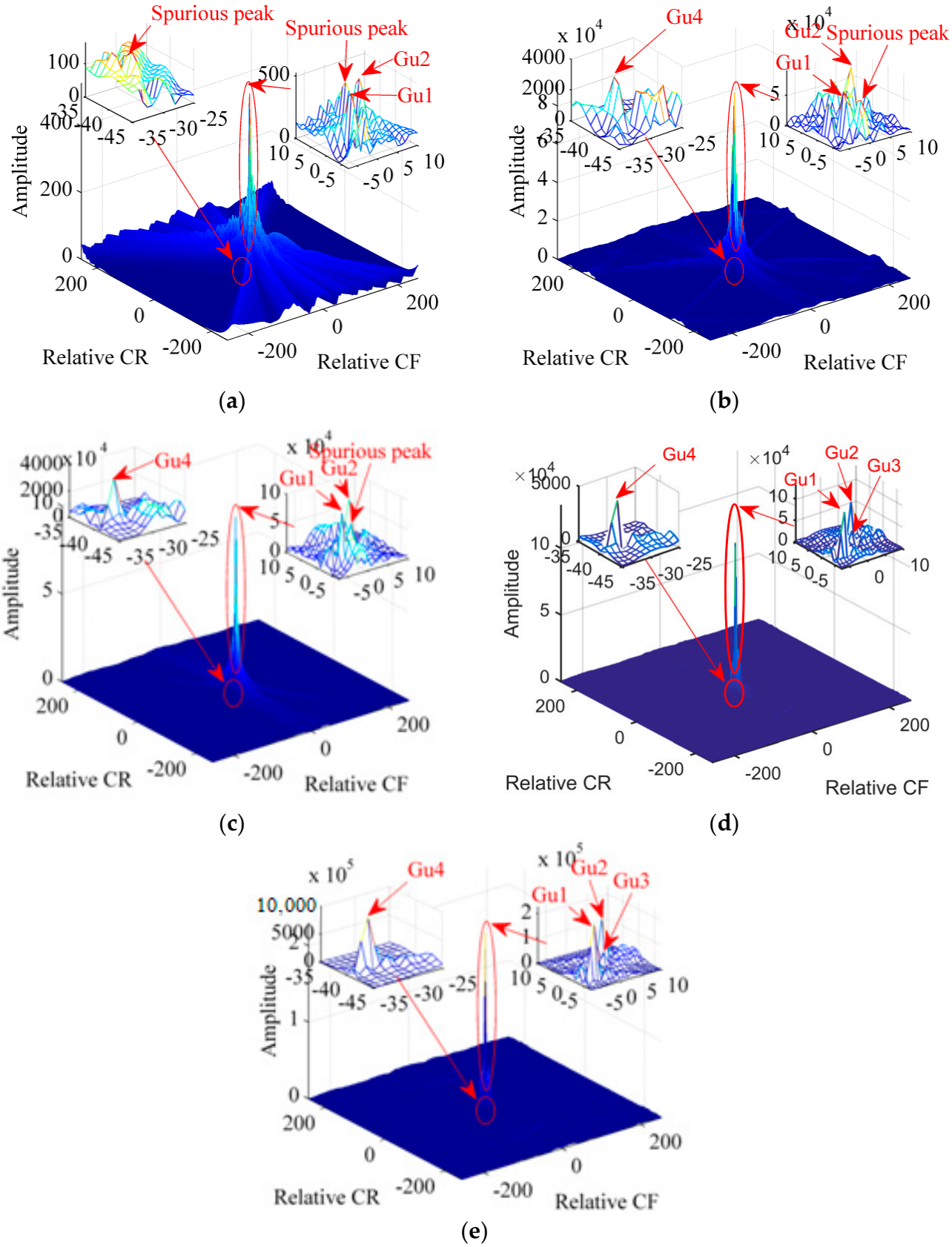

Figure 8. LFM signals with different amplitudes (of large differences). (**a**) Result of the ML method. (**b**) Result of the WHT. (**c**) Result of the LVD. (**d**) Result of the PCFCRD. (**e**) Result of the ImLVD.

Gu1, *Gu2* and *Gu3* are close to each other. Since resolutions and PSLs of the ML method, WHT and LVD are low, and the WHT and LVD have the cross term interference, the spurious peak appears instead of the weak *Gu3* in Figure 8a–c. In Figure 8d,e obtained with the PCFCRD and ImLVD, four real signals appear without spurious peaks due to the high cross-term suppression, resolution and PSL. Processing results shown in Figure 8 demonstrate that the ImLVD has the obvious superiority under the LFM signal with different amplitudes (of large differences). It is interesting to find that, in Figure 8a obtained via the ML method, a spurious peak appears instead of *Gu4*, while *Gu4* are successfully detected by other algorithms in Figure 8b–d. This may indicate that the cross term may sometimes benefit the auto term detection. We will study this phenomenon in the future.

4.3. Noisy Multicomponent LFM Signals

In this subsection, we use a numerical example to evaluate the anti-noise performance of the ImLVD for noisy multicomponent LFM signals analysis.

Numerical Example 3. *We consider three LFM signals, Hu1, Hu2 and Hu3. Signal parameters are listed in Table 6, and constant delays of the PCFCRD and ImLVD are set to 2 s. Three signals have the same amplitude and are far away from each other. Therefore, if we directly apply the ML method, WHT, LVD, PCFCRD and ImLVD to them, only the noise can induce spurious peaks. Here, we contaminate the signal with the complex white Gaussian noise, and the* SNR_{in} *is* -12 *dB. Figure 9a–e correspond to results of the ML method, WHT, LVD, PCFCRD and ImLVD, respectively.*

Table 6. Signal Parameters.

Sampling Frequency F_s	**300 Hz**	**Signal Length** N	**600**
Parameters of *Hu1*	$A_1 = 1$	$a_{1,1}$ = 60 Hz	$a_{2,1}$ = 40 Hz/s
Parameters of *Hu2*	$A_2 = 1$	$a_{1,2}$ = 2 Hz	$a_{2,2}$ = 2 Hz/s
Parameters of *Hu3*	$A_3 = 1$	$a_{1,3} = -40$ Hz	$a_{2,3} = -30$ Hz/s

It is clearly seen from Figure 9a–c that the signal energy is submerged by the random noise, and spurious peaks appear. However, in Figure 9d,e, the signal energy is larger than that of the noise and no spurious peak appears. Simulation results in Figure 9 demonstrate that the PCFCRD and ImLVD have higher integration SNR gain than the ML method, WHT and LVD, and are more suitable for noisy multicomponent LFM signal analysis.

Note that, in Figures 8 and 9, the PCFCRD and ImLVD obtain similar results. However, analyses and simulations in Section 4 do indicate that the ImLVD outperforms the PCFCRD in the cross-term suppression, PSL and anti-noise performance. Therefore, under some extreme situations, results of the ImLVD must be better than those of the PCFCRD. In addition, the PCFCRD is based on the time-CR transform, and the integration variable in the integrant is non-uniform. In conclusion, compared to the ML method, WHT, PCFCRD and LVD, the ImLVD is more suitable for realistic applications.

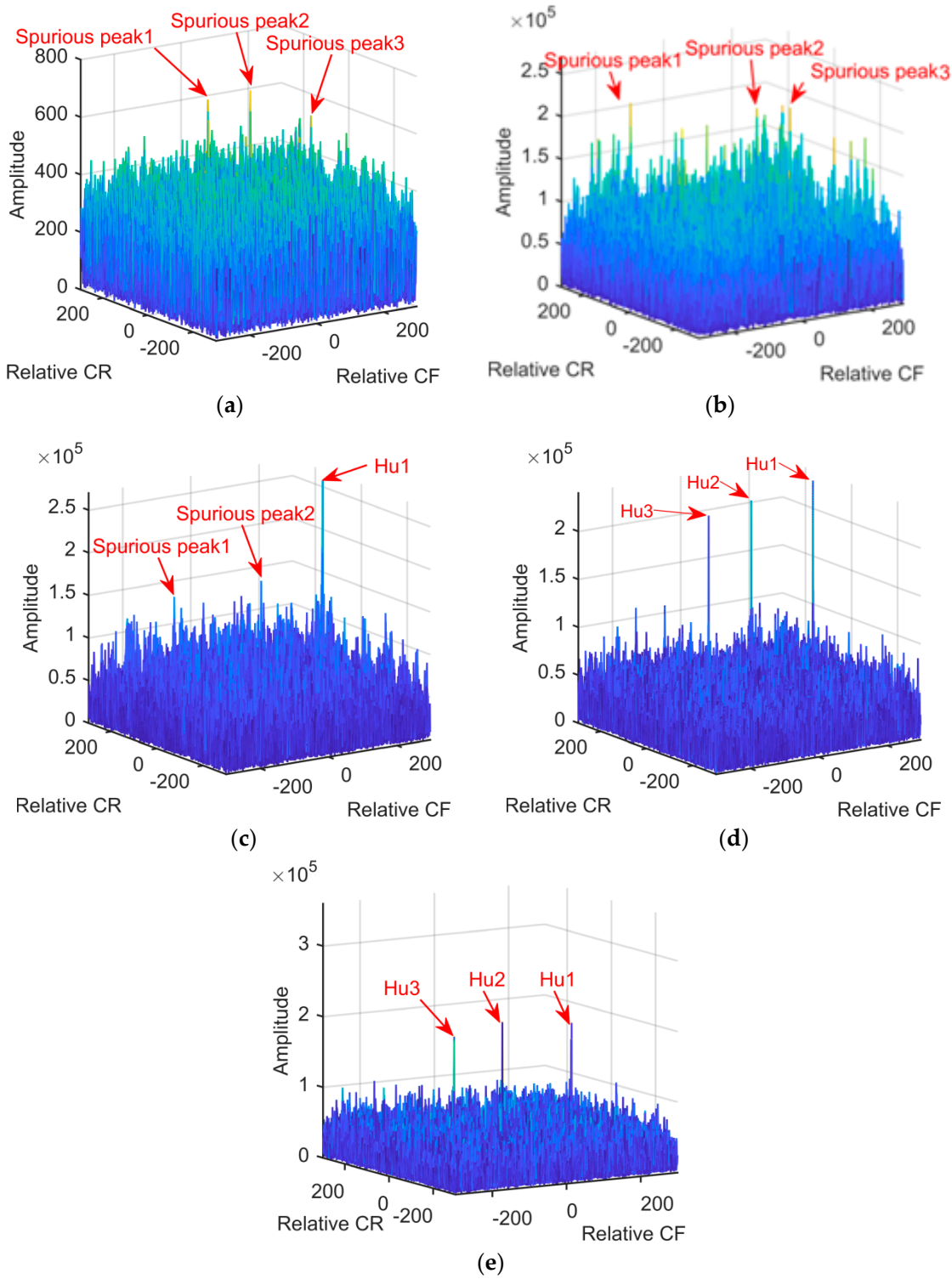

Figure 9. Comparison of the integration SNR gain under noisy multicomponent LFM signals. (**a**) Result of the ML method. (**b**) Result of the WHT. (**c**) Result of the LVD. (**d**) Result of the PCFCRD. (**e**) Result of the ImLVD.

5. Conclusions and Future Work

Two contributions can be obtained from this paper, including the ImLVD and further study of the introduced constant delay. With theoretical analyses and illustrative examples, compared to the ML method, WHT, LVD and PCFCRD, the ImLVD has higher cross-term suppression, resolution, PSL and anti-noise performance without the non-uniform

integration variable. Finally, three numerical examples are used to validate the practicability of the ImLVD. In this paper, the quantitative influences of the constant delay on the cross-term suppression, resolution, PSL and anti-noise performance are obtained by using theoretical analyses of the ImLVD, which is useful for future applications of the constant delay introduction.

Many investigations have been carried out for noisy multicomponent LFM signals analysis in radar signal processing, while physical attributes determine that, no matter how the CFCRAT works, some drawbacks are inherent and cannot be overcame. With the analyses and simulations in this paper, we find that the introduced constant delay is helpful for the research into the CFCRAT. In the future work, we will continue the study on the constant delay introduction, especially its applications in radar detection and imaging.

Author Contributions: Conceptualization, K.Y.; Methodology, X.L.; Software, Y.L.; Validation, J.Z. All authors have read and agreed to the published version of the manuscript.

Funding: This research received no external funding.

Data Availability Statement: The data presented in this study are available on request from the corresponding author.

Conflicts of Interest: The authors declare no conflict of interest.

Appendix A

This appendix presents the fast implementation of the ImLVD based on the FFT- and IFFT-based CZT. To formulate the implementation, we consider a noise-free LFM signal, whose discrete form is expressed as

$$s_1(m) = A_1 \exp\left\{ j2\pi \left[a_{1,1} m T_s + \frac{1}{2} a_{2,1} (m T_s)^2 \right] \right\} \tag{A1}$$

With $s_1(m)$, we can write the discrete form of $R_3(t, \tau)$ defined in (11) as

$$R_3(m,k) = G_1 \exp(j4\pi a_{1,1} k T_s) \exp[j2\pi a_{2,1} (2kT_s + h) m T_s] \tag{A2}$$

where $G_1 = A_1^2 \exp(j2\pi a_{1,1} h)$.

The implementation of the ImLVD in (12) can be separated into two steps, the inner Fourier transform and the outer Fourier transform. The discrete form of the inner Fourier transform can be written as

$$\hbar(m_r, k) = \sum_m R_3(m,k) \exp\left[-j2\pi \frac{m_r}{N} (2kT_s + h) m \right] (2kT_s + h) \tag{A3}$$

where $m_r = -[N/2], -[N/2]+1, \ldots, [(N-1)/2]$ corresponds to the discrete frequency domain.

Based on the characteristic of the Formula (A3), we rewrite it as

$$\hbar(m_r, k) = \exp\left[-j\pi \frac{m_r^2}{N} (2kT_s + h) \right] (2kT_s + h) \sum_m R_3(m,k) \exp\left[-j\pi \frac{m^2}{N} (2kT_s + h) \right] \exp\left[j\pi \frac{(m_r - m)^2}{N} (2kT_s + h) \right] \tag{A4}$$

The summation in (A4) can be regarded as a convolution. So we can implement it with the FFT and IFFT.

$$\hbar(m_r, k) = \varpi(m_r, k) \mathrm{FFT}_m \left\{ \mathrm{IFFT}_{m_r} \left\{ \exp\left[j\pi \frac{{m_r}^2}{N} (2kT_s + h) \right] \right\} \mathrm{IFFT}_{m_r} \left\{ R_3(m_r, k) \exp\left[-j\pi \frac{{m_r}^2}{N} (2kT_s + h) \right] \right\} \right\} \tag{A5}$$

where $\varpi(m_r,k) = \exp\left[-j\pi\frac{m_r^2}{N}(2kT_s+h)\right](2kT_s+h)$. Note that $\varpi(m_r,k) = \exp\left[-j\pi\frac{m_r^2}{N}(2kT_s+h)\right]$ for the implementation of the LVD in [20]. Since $\varpi(m_r,k)$ can be calculated in advance, this difference has no influence on the computational cost compared to that of the LVD.

Subsequently, the IFFT can be used to complete the inner Fourier transform. After the FFT- and IFFT-based implementation, we obtain

$$\hbar(m_r,k) = G_1' \exp(j4\pi a_{1,1} k T_s)\mathrm{sinc}\left[\frac{(T+h)^2}{2}\left(\frac{m_r}{NT_s} - a_{2,p}\right)\right] \tag{A6}$$

where G_1' denotes the amplitude. It is worthwhile noting that Equations (A4) and (A5) are used to illustrate how we speed up the computation from Equation (A3) to Equation (A6).

The second step, the discrete form of the outer Fourier transform, can be written as

$$\begin{aligned}\mathrm{ImLVD}\left(k_f, m_r\right) &= \sum_k \hbar(m_r,k)\exp\left(-j2\pi\frac{k_f}{N}k\right)\\ &= \mathrm{FFT}_k\{\hbar(m_r,k)\}\end{aligned} \tag{A7}$$

where $k_f = -[N/2], -[N/2]+1, \ldots, [(N-1)/2]$ corresponds to the discrete frequency domain.

Substituting $\hbar(m_r,k)$ in (A6) into (A7), we have

$$\mathrm{ImLVD}\left(k_f, m_r\right) = K_p'''\,\mathrm{sinc}\left[\frac{T}{2}\left(\frac{k_f}{NT_s} - 2a_{1,p}\right)\right]\mathrm{sinc}\left[\frac{(T+h)^2}{2}\left(\frac{m_r}{NT_s} - a_{2,p}\right)\right] \tag{A8}$$

Above is the ImLVD implementation by using the FFT- and IFFT-based CZT.

References

1. Peleg, S.; Porat, B. The Cramer-Rao lower bound for signals with constant amplitude and polynomial phase. *IEEE Trans. Aerosp. Electron. Syst.* **1991**, *39*, 749–752. [CrossRef]
2. Aldimashki, O.; Serbes, A. Performance of Chirp Parameter Estimation in the Fractional Fourier Domains and an Algorithm for Fast Chirp-Rate Estimation. *IEEE Trans. Aerosp. Electron. Syst.* **2020**, *56*, 3685–3700. [CrossRef]
3. Yang, N.-C.; Yang, J.-M. Fault Classification in Distribution Systems Using Deep Learning with Data Preprocessing Methods Based on Fast Dynamic Time Warping and Short-Time Fourier Transform. *IEEE Access* **2023**, *11*, 63612–63622. [CrossRef]
4. Liang, C.; Teng, Z.; Li, J.; Yao, W.; Wang, L.; He, Q.; Hu, S. Improved S-Transform for Time-Frequency Analysis for Power Quality Disturbances. *IEEE Trans. Power Deliv.* **2022**, *37*, 2942–2952. [CrossRef]
5. Boashash, B. *Time-Frequency Signal Analysis and Processing: A Comprehensive Reference*; Academic Press: Cambridge, MA, USA, 2015.
6. Yu, Y.; Liu, L.; Zhou, Z.; Du, Z.; Jiao, C. Identification Method for Pulse Wave Resulted from Fault Transient of Overhead Transmission Line. *IEEE Access* **2023**, *11*, 32006–32017. [CrossRef]
7. Zhang, H.; Shan, T.; Liu, S.; Tao, R. Optimized sparse fractional Fourier transform: Principle and performance analysis. *Signal Process.* **2020**, *174*, 107646. [CrossRef]
8. Liu, S.; Zhang, H.; Shan, T.; Huang, Y. Efficient radar detection of weak maneuvering targets using a coarse-to-fine strategy. *IET Radar Sonar Navig.* **2021**, *15*, 181–193. [CrossRef]
9. Peng, Y.; Ding, Y.; Zhang, J.; Jin, B.; Chen, Y. Target Trajectory Estimation Algorithm Based on Time–Frequency Enhancement. *IEEE Trans. Instrum. Meas.* **2022**, *72*, 8500807. [CrossRef]
10. Salata, G.; Cenkeramaddi, L.R.; Huynh, V.K.; Robbersmyr, K.G.; Jha, A. Time–Frequency Analysis and Fault Prediction of Motor Bearings Using Millimeter-Wave Radar. *IEEE Sens. J.* **2023**, *23*, 18718–18728. [CrossRef]
11. Shi, J.; Chen, G.; Zhao, Y.; Tao, R. Synchrosqueezed Fractional Wavelet Transform: A New High-Resolution Time-Frequency Representation. *IEEE Trans. Signal Process.* **2023**, *71*, 264–278. [CrossRef]
12. Luo, S.; Bi, G.; Lv, X.; Hu, F. Performance analysis on Lv distribution and its applications. *Digit. Signal Process.* **2013**, *23*, 797–807. [CrossRef]
13. Qiu, S.; Sheng, W.; Ma, X.; Kirubarajan, T. A Maximum Likelihood Method for Joint DOA and Polarization Estimation Based on Manifold Separation. *IEEE Trans. Aerosp. Electron. Syst.* **2021**, *57*, 2481–2500. [CrossRef]
14. Xia, X.-G. Discrete chirp-Fourier transform and its application to chirp rate estimation. *IEEE Trans. Signal Process.* **2000**, *48*, 3122–3133. [CrossRef] [PubMed]
15. Guo, X.; Sun, H.-B.; Wang, S.-L.; Liu, G.-S. Comments on Discrete Chirp-Fourier Transform and its Application to Chirp Rate Estimation. *IEEE Trans. Signal Process.* **2002**, *50*, 3115–3116.
16. Koç, A.; Bartan, B.; Ozaktas, H.M. Discrete Linear Canonical Transform Based on Hyperdifferential Operators. *IEEE Trans. Signal Process.* **2019**, *67*, 2237–2248. [CrossRef]

17. Lv, X.; Bi, G.; Wang, C.; Xing, M. Lv's distribution: Principle, implementation, properties, and performance. *IEEE Trans. Signal Process.* **2011**, *59*, 3576–3591. [CrossRef]
18. Sun, Y.; Willett, P. Hough transform for long chirp detection. *IEEE Trans. Aerosp. Electron. Syst.* **2002**, *38*, 553–569. [CrossRef]
19. Wang, H.; Fan, X.; Chen, Y.; Yang, Y. Wigner-Hough transform based on slice's entropy and its application to multi-LFM signal detection. *J. Syst. Eng. Electron.* **2017**, *28*, 634–642.
20. Guner, K.K.; Gulum, T.O.; Erkmen, B. FPGA-Based Wigner–Hough Transform System for Detection and Parameter Extraction of LPI Radar LFMCW Signals. *IEEE Trans. Instrum. Meas.* **2021**, *70*, 2003515. [CrossRef]
21. Kiang, C.-W.; Kiang, J.-F. Imaging on Underwater Moving Targets with Multistatic Synthetic Aperture Sonar. *IEEE Trans. Geosci. Remote Sens.* **2022**, *60*, 4211218. [CrossRef]
22. Liu, Q.; Gily, B.; Fok, M.P. Adaptive Photonic Microwave Instantaneous Frequency Estimation Using Machine Learning. *IEEE Photonics Technol. Lett.* **2021**, *33*, 1511–1514. [CrossRef]
23. O'Shea, P. A fast algorithm for estimating the parameters of a quadratic FM signal. *IEEE Trans. Signal Process.* **2004**, *52*, 385–393. [CrossRef]
24. O'Neill, J.C.; Flandrin, P. Virtues and vices of quadratic time-frequency distribution. *IEEE Trans. Signal Process.* **2000**, *48*, 2641–2650. [CrossRef]
25. O'Shea, P. Improving polynomial phase parameter estimation by using nonuniformly spaced signal sample methods. *IEEE Trans. Signal Process.* **2012**, *60*, 3405–3414. [CrossRef]
26. Zuo, L.; Li, M.; Liu, Z.; Ma, L. A high-resolution time-frequency rate representation and the cross-term sup-pression. *IEEE Trans. Signal Process.* **2016**, *64*, 2463–2474. [CrossRef]
27. Simeunović, M.; Djurović, I. Non-uniform sampled cubic phase function. *Signal Process.* **2014**, *101*, 99–103. [CrossRef]
28. Wang, P.; Yang, J. Multicomponent chirp signals analysis using product cubic phase function. *Digit. Signal Process.* **2006**, *16*, 654–669. [CrossRef]
29. Li, D.; Zhan, M.; Su, J.; Liu, H.; Zhang, X.; Liao, G. Performances Analysis of Coherently Integrated CPF for LFM Signal Under Low SNR and Its Application to Ground Moving Target Imaging. *IEEE Trans. Geosci. Remote Sens.* **2017**, *55*, 6402–6419. [CrossRef]
30. Li, X.; Kong, L.; Cui, G.; Yi, W.; Yang, Y. ISAR imaging of maneuvering target with complex motions based on ACCF–LVD. *Digit. Signal Process.* **2015**, *46*, 191–200. [CrossRef]
31. Bao, M.; Jia, B.; Li, Y.; Guo, L.; Xing, M. Coherent Integration for Maneuvering Target Detection at Low SNR Based on Radon-General Linear Chirplet Transform. *IEEE Geosci. Remote Sens. Lett.* **2022**, *19*, 4027505. [CrossRef]
32. Byram, B.; Jakovljevic, M. Ultrasonic multipath and beamforming clutter reduction: A chirp model approach. *IEEE Trans. Ultrason. Ferroelectr. Freq. Control* **2014**, *61*, 428–440. [CrossRef] [PubMed]
33. Byram, B.; Dei, K.; Tierney, J.; Dumont, D. A model and regularization scheme for ultrasonic beamforming clutter reduction. *IEEE Trans. Ultrason. Ferroelectr. Freq. Control* **2015**, *62*, 1913–1927. [CrossRef] [PubMed]
34. Zheng, J.; Su, T.; Liu, Q.H.; Zhang, L.; Zhu, W. Fast parameter estimation algorithm for cubic phase signal based on quantifying effects of doppler frequency shift. *Prog. Electromagn. Res.* **2013**, *142*, 57–74. [CrossRef]
35. Zhu, D.; Li, Y.; Zhu, Z. A keystone transform without interpolation for SAR ground moving-target imaging. *IEEE Geosci. Remote Sens. Lett.* **2007**, *4*, 18–22. [CrossRef]
36. Li, X.; Xing, M.; Xia, X.-G.; Sun, G.-C.; Liang, Y.; Bao, Z. Simultaneous Stationary Scene Imaging and Ground Moving Target Indication for High-Resolution Wide-Swath SAR System. *IEEE Trans. Geosci. Remote Sens.* **2016**, *54*, 4224–4239. [CrossRef]
37. Zheng, J.; Liu, H.; Liu, Q.H. Parameterized centroid frequency-chirp rate distribution for LFM signal analysis and mechanisms of constant delay introduction. *IEEE Trans. Signal Process.* **2017**, *65*, 6435–6447. [CrossRef]